Texas A&M University
Mechanical Engineering Department
Turbomachinery Laboratory
Tribology Group

Rotordynamic Measurements on a High Temperature Rotor Supported on Gas Foil Bearings

Research Progress Report to the TAMU Turbomachinery Research Consortium

TRC-B&C-3-08

by

Tae Ho Kim
Post-doctoral Research Associate

Luis San Andrés
Mast-Childs Professor
Principal Investigator

June 2008

This material is based upon work supported by NASA Research Announcement NNH06ZEA001N-SSRW2, Fundamental Aeronautics: Subsonic Rotary Wing Project 2

Prediction of Foil Bearing Performance: A Computational Model Anchored to Test Data
Texas Engineering Experiment Station Project # 32525/39600/ME
TRC Project TEES# 32513/1519C4

EXECUTIVE SUMMARY

Rotordynamic Measurements on a High Temperature Rotor Supported on Gas Foil Bearings

TRC-B&C-3-08

Exhaustive experimentation and accurate model prediction will lead to successful implementation of gas foil bearings (GFBs) into high temperature applications. This report presents rotordynamic measurements in a gas bearing test rig revamped for high temperature operation. The tests aim to determine the effect of temperature on the system performance. An electric cartridge heater loosely installed inside the rotor acts as a heat source. Two GFBs support a hollow rotor, one of the GFB (drive end) is Teflon® coated while the other (free end) is uncoated. K-type thermocouples measure the GFB cartridge temperatures, and infrared thermometers measure the shaft and bearing support temperatures. If needed, an axial air flow cools the rotor and GFBs.

Increasing heater temperatures, as high as 132 °C, are set. Long times, on the order of hours, are required to reach thermal equilibrium. As expected, bearing temperatures increase as the heater temperature increases and as the rotating speed increases. Rotor speed-up tests to 26 krpm without shaft heating show that the rotor amplitude of motions drops suddenly just above the rotor-bearing system critical speed, thus evidencing a nonlinearity (hardening effect) of the foil bearings. At the hottest condition, heater at 132 °C, the rotor peak amplitude of motion decreases dramatically and shows a typical linear response without jumps. Rotor speed coastdown tests from 26 krpm show the system critical speed increases by 1.5 krpm as the heater temperature increases from 22 °C to 132 °C. In addition, while coasting down, from 26 krpm to ~ 8 krpm, rotor speed decays exponentially as time elapses, thus evidencing operation with “viscous” drag.

Measurements of bearing and shaft temperatures show the limited effectiveness of the cooling flow stream; i.e. too large flow rates are needed to reduce the bearing temperature a few degrees; in particular for high shaft temperatures. Hence, adequate thermal management in foil bearings remains an issue of engineering importance. Later developments must focus on bearing materials and devising adequate means of conduction and disposal of thermal energy through the bearing cartridge.

Note from Editor: TRC-B&C-3-08 reproduces Quarter 3 Progress Report to NASA GRC (June 2008). Current report edited five times prior to its release to TRC members.

TABLE OF CONTENTS

LIST OF TABLES

LIST OF FIGURES

I. INTRODUCTION

Application of gas foil bearings (GFBs) into midsize gas turbine engines, operating in high temperature environment, demands reliable performance measurements and predictions [1]. GFBs are known for their low drag and ability to tolerate high levels of vibrations, including transient rubs and shaft misalignment, static and dynamic, thus increasing system efficiency and operating life [1,2]. The forced performance of a GFB depends upon the material properties and geometrical configuration of its support structure (the top foil and bump strip layers), as well as the hydrodynamic film pressure generated within the bearing clearance. Engineered solid lubricant coatings determine early rotor lift-off, reduced power losses (drag torque) during rotor-bearing system start-up and shut-down conditions, and reduce wear of components during these transient operational events [1,3]. Often, a cooling gas flow is forced through the foil bearing underlying structure to carry away heat generated by a hot component, for example. This highly effective cooling method [4,5] controls thermal growth of components and changes in material properties, reduces thermal gradients and prevents hot spots in the bearings; hence extending their life [4]. With an adequate supply of cooling flow into a GFB supporting the hot end of a micro gas turbine, Ref. [6] describes successful endurance tests conducted to 120 krpm at an operating temperature of 800 °C.

The report presents rotordynamic measurements on a rotor supported on GFBs. An electric cartridge heater loosely fitted inside a hollow rotor heats the rotating shaft. K-type thermocouples and infrared thermometers measure temperatures of test GFBs (bearing cartridge inside through axial slots and its outer surface), rotating shaft, and bearing support. Rotor speed-up and coastdown tests evidence the effects of shaft temperature on the rotordynamic performance of the test GFBs.

II. LITERATURE REVIEW

In spite of the progress advanced in analysis, gas foil bearing design is still largely empirical, each foil bearing being a custom piece of hardware, with resulting variability even in identical units, and limited scalability [7]. In the last few years, research at NASA GRC has been instrumental to advance the state of art in GFB technology, in particular for coatings applicable to high temperature environments. The literature review details past experimental work on the performance of GFBs operating at high temperatures.

DellaCorte [8] introduces a test rig to evaluate the static load and torque of GFBs for operation at high speeds and realistic temperatures, to 650 ºC (1200 ºF), with intended application to gas turbine engines. A furnace, holding test journal and GFB altogether inside, heats the ambient air. Measured toque versus rotor speed reveals start up (or shut down) operation with a mixed boundary lubrication region and, upon journal lift off, a pure hydrodynamic region. In general, GFB torque is proportional to applied static load, with load capacity being a linear function of rotor speed. The author reports a decrease of ~30 % in load capacity for a GFB tested at increasing temperatures ranging from 25ºC to 650 ºC.

DellaCorte and co-workers [9] perform GFBs durability tests with a PS304 coating (high temperature solid lubricant) for operation between 25 ºC and 650 ºC. The GFB experiences sliding contact (rubbing) with the shaft during initial start up and shut down operations. The PS304 coating applied on the shaft protected the foil surface from wear. A 100,000 start/stop cycles journal lift-off test results reveals that wear is proportional to the applied static load. The research demonstrates a suitable static performance of GFBs in moderate to high temperature applications.

DellaCorte et al. [10] conduct load capacity tests on GFBs with various combinations of shaft coatings and top foil coatings. Bearings with various coating deposition processes (sprayed, heat treated, ground, and polished) are tested to compare their ability to improve GFB load capacity. PS304 coatings on the shaft were over coated with either polyimide or Molybdenum Disulphide (MoS_2) for additional solid lubrication. Test results reveal that an effective solid lubricant film, such as MoS_2, must be present on the top foil surface to achieve a satisfactory load capacity upon initial installation of a PS304 coated shaft, i.e. an as-grounded PS304 coated shaft. Non-galling wear resistant coatings such as PS304 on the shaft and Al-Cu on the foil enhance performance even further. To prevent bearing failure, the material selected must not produce large, hard debris particles as was the case with the polyimide, especially upon thermal decomposition (burn-off). Thus, the combination of a PS304 coated shaft with sacrificial MoS_2 running against Al-Cu coated top foil works synergistically to give a maximum load capacity from first installation to fully run-in GFB operations.

Bauman [5] introduces a thrust GFB test rig for use in oil-free gas turbines being developed at NASA. The test rotor supported on a thrust GFB and two journal GFBs operates to a top speed of 80,000 rpm and temperatures up to 650 ºC. A hydrostatic loader piston provides an axial load

to the shaft, and a magnetic thrust bearing counteracts the test thrust GFB loads ensuring a steady motion of the thrust runner. Cooling air is supplied into the test rig housing to carry away waste heat from the magnetic thrust bearing as well as the heat conducted from a hot turbine to the journal GFB. Note that adequate thermal management is necessary when incorporating GFBs into high temperature applications, such as in a gas turbine engine [3]. The axially fed cooling flow prevents hot-spots in the GFB and extends its life. Measurement parameters of the test rig include bearing torque, load capacity, and bearing temperature, which will be used to validate computational models of GFBs.

Howard et al. [11,12] perform impact tests on a floating GFB and identify its dynamic direct stiffness and damping for operation at increasing temperatures, static load, shaft speed and temperature. In general, GFB stiffness increases with applied load and decreases slightly with rotor speed. Free response decay test data are compared with both exponential (viscous damping) and linear (Coulomb damping) decays to realize the dominant energy dissipation mechanism. Experiments demonstrate that at high temperatures and low static loads, the gas film is soft (compared to the foil structure) thus showing viscous damping behavior. Conversely, at low temperatures and high static loads the bearing behaves as a structural system with dry friction, since the gas film is much stiffer than the foil structure. In general, GFB load capacity and stiffness reduce considerably as the operating temperature increases.

Lee et al. [13] conduct experiments to evaluate the structural stiffness and equivalent viscous damping of a foil sub-structure at increasing temperatures. An electromagnetic shaker excites a bump strip layer supporting a flat top foil, and a fiber optic displacement sensor measures the bump deflections, while a thermal system heats the bump strip layer. Experimentally derived stiffness and damping coefficients, for increasing temperatures (up to 500 º C), validate a two dimensional FE model of the foil sub-structure incorporating thermal effects.

Lubell et al. [3] evaluate high temperature coatings for GFBs used in oil-free micro gas turbine engines. The solid lubricant not only reduces friction torque during the start-up and shut-down of turbomachinery supported on GFBs, but also prevents failures related to coating degradation of the shaft and bearings at high temperatures, well above 500 ºC (930 ºF). The paper describes a micro gas turbine engine test with a shaft coated using PS304 developed by NASA. The shaft is supported on a GFB in the hot section. During endurance engine tests, two coating related failures were recorded. Subsequently, new coating procedures were adopted, i.e.

plasma spray on the shaft with an oblique angle at both shaft end locations and simple heat treatment of coated parts prior to final surface grinding. These procedures coat the shaft surface uniformly and enhance the coating adherence, thus improving the coating micro-structural stability characteristics at high temperature operation. Further engine tests demonstrated successful operation at 500°C (930°F) for over 2,500 hours and 2,900 start-stop cycles without damage or loss of performance.

Salehi et al. [14] measure the load capacity of a GFB with its diameter and axial length of 100 mm in room temperature environment. A hydraulic loading system provide static loads on the bearing cartridge floating on a rotor spinning at maximum speed of 36 krpm. The experiment also measures temperature-rises of the cooling flow passing through the GFB by measuring the flow inlet and outlet temperatures using thermocouples installed on the outer (or back) side of the top foil. Test results show that the GFB has a greater temperature in the static load direction rather than in the opposite direction. The temperature grows with increasing rotor speed and static load. A comparison of the predicted temperature-rise of the cooling flow to the experimental measurement shows good agreement within a deviation of ~20 %, i.e., the predicted temperatures are slightly lower than test.

Adequate thermal management aids to prevent GFBs from encountering thermal seizure, thus maintaining a desired load capacity and stability [3-6]. Implementing a side end cooling flow into GFBs, a *direct* cooling method [5], controls thermal growth of components and changes in material properties, diminishes the severity of thermal gradients, and prevents hot spots in the bearings; hence extending their life, for example. Radil et al. [4] evaluate experimentally the efficiency of an *indirect* cooling method that forces a gas stream through a hollow rotor. This apparently less efficient method, however, has the advantage of controlling shaft surface thermal gradients and reducing shaft thermal growth over a long section of a turbine rotor, for example.

III. DESCRIPTION OF ROTORDYNAMIC TEST RIG

Rotordynamic response measurements are conducted on a hollow rotor supported on GFBs[1] for increasing rotor surface temperatures and for increasing rotor speeds. Figure 1 shows the GFB test rig for the rotordynamic experiments. The rotordynamic test rig in Refs. [15,16] is

[1] See Appendix A for a description of the test GFBs.

revamped using an electric cartridge heater, installed inside the rotating hollow rotor with a gap of 1.7 mm, and acting as a heat source to the shaft.

A router AC motor, 1.49 kW (2.0 HP) with maximum speed of 25 krpm drives the rotor supported on test GFBs with diameter and axial length of 38.1 mm through a flexible coupling. Two pairs of orthogonally positioned eddy current sensors located at both rotor drive and free ends record the lateral rotor motions along the horizontal and vertical planes, as detailed in Ref. [16]. The test rig housing holds two test GFBs and contains an internal duct to supply a cooling air flow, if needed. The pressurized air supplied at rotor midspan forces a cooling flow through the test GFBs. A gas flow meter (max. 100 liter/min) measures the air cooling flow rate.

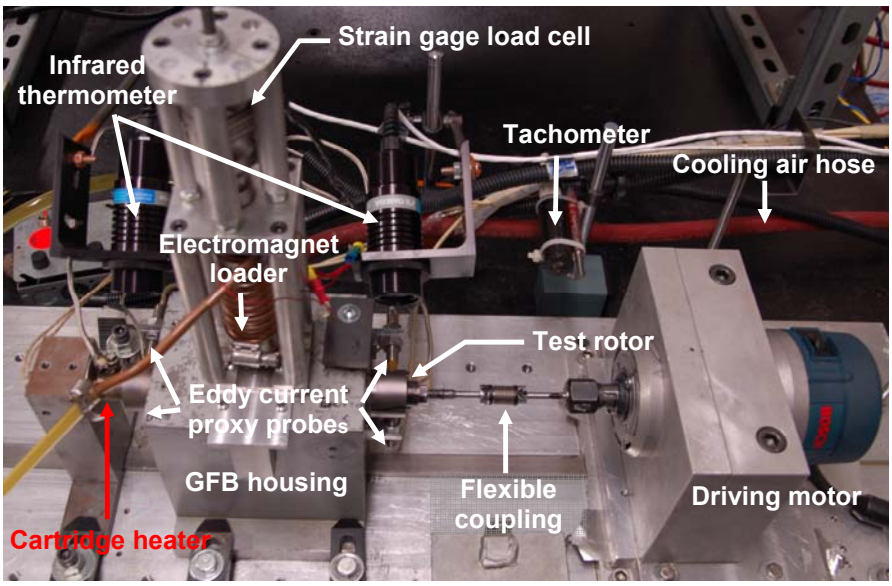

Figure 1. Test rig for rotordynamic tests of a rotor supported on GFBs with cartridge heater and instrumentation for operation at high temperature

The electric heater has a heated section with axial length of 171 mm and diameter of 22 mm. A controller and a switching device set the heater surface temperature at one location. The cartridge heater is calibrated in room temperature environment (~ 22°) using a thermocouple (Type K) fixed on the one end of the heater and an infrared thermometer measuring the heater surface temperatures along the axial length. The thermocouple provides a nominal heater temperature to the controller. Appendix B shows the measured surface temperatures of the heater along the axial length as the (nominal) controlled temperature increases. In general, the heat is not uniformly distributed along the axial length; a distinct thermal gradient is apparent.

IV. EXPERIMENTAL PROCEDURE

Figure 2 shows a schematic view of the rotordynamic test rig with the cartridge heater and instrumentation for measurement of test rig components. In the figure, numbers 1 - 4 in circles denote the locations of temperature measurements. (1) Five K-type thermocouples, installed in the drive end GFB cartridge though five axial slots, measure the temperatures at the bearing mid-plane along its circumference. (2) Two K-type thermocouples, each installed at the outboard of the drive or free end GFB outer surface (OD), measure the bearing outer surface temperatures. (3) Two infrared thermometers measure the drive and free end rotor surface temperatures. (4) An infrared thermometer gun measures the drive and free end bearing support (housing) surface temperatures.

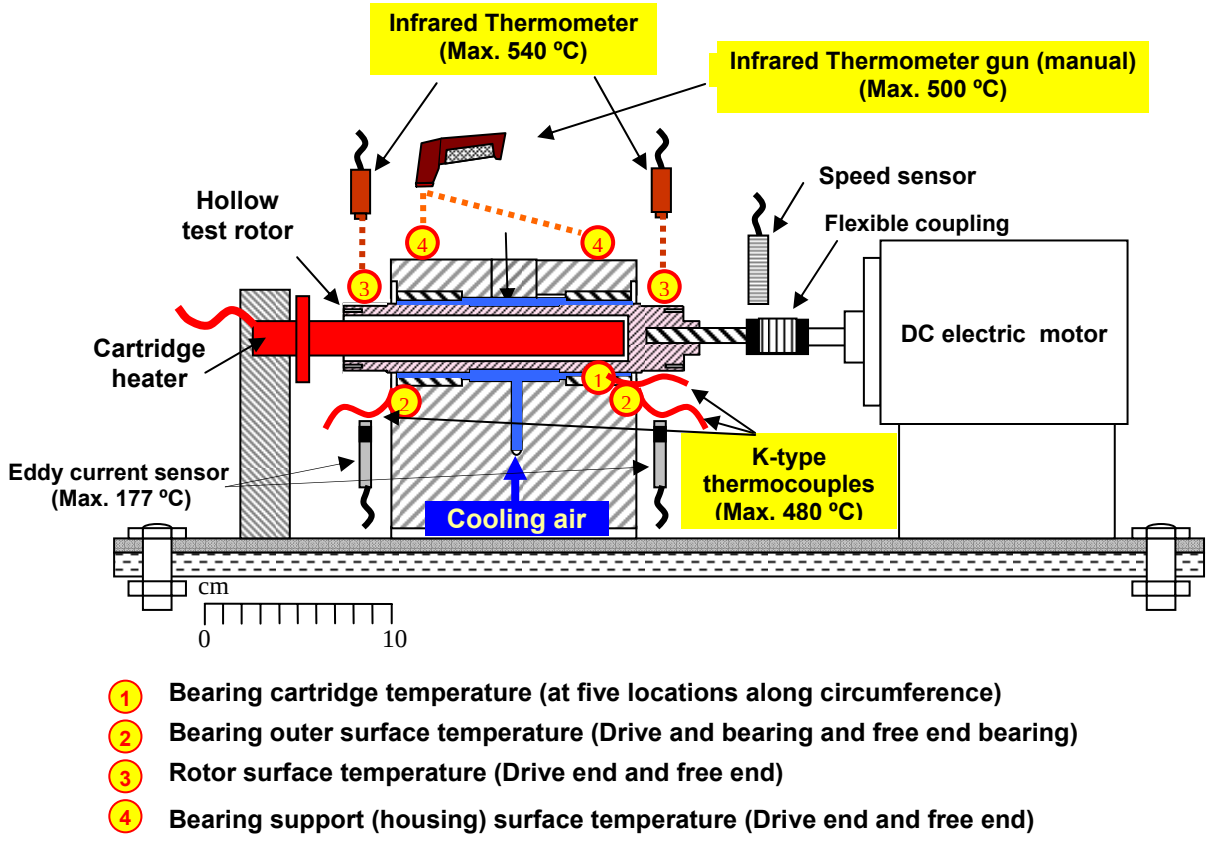

Figure 2. Schematic view of rotordynamic test rig with cartridge heater and instrumentation for operation at high temperature. Numbers in circles denote locations of temperature measurement

Figure 3 illustrates a cross-section view of the drive end GFB with five thermocouples placed in machined axial slots at the circumferential locations (Θ = 22°, 94°, 166°, 238°, 310°) at the bearing mid-plane. Note that the angles for the five thermocouples correspond with those for the second bump (from the free end) of five bump strip layers, each with five bumps[2]. The bearing cartridge temperatures, around the circumference, are representative of the GFB inner surface (ID) temperatures.

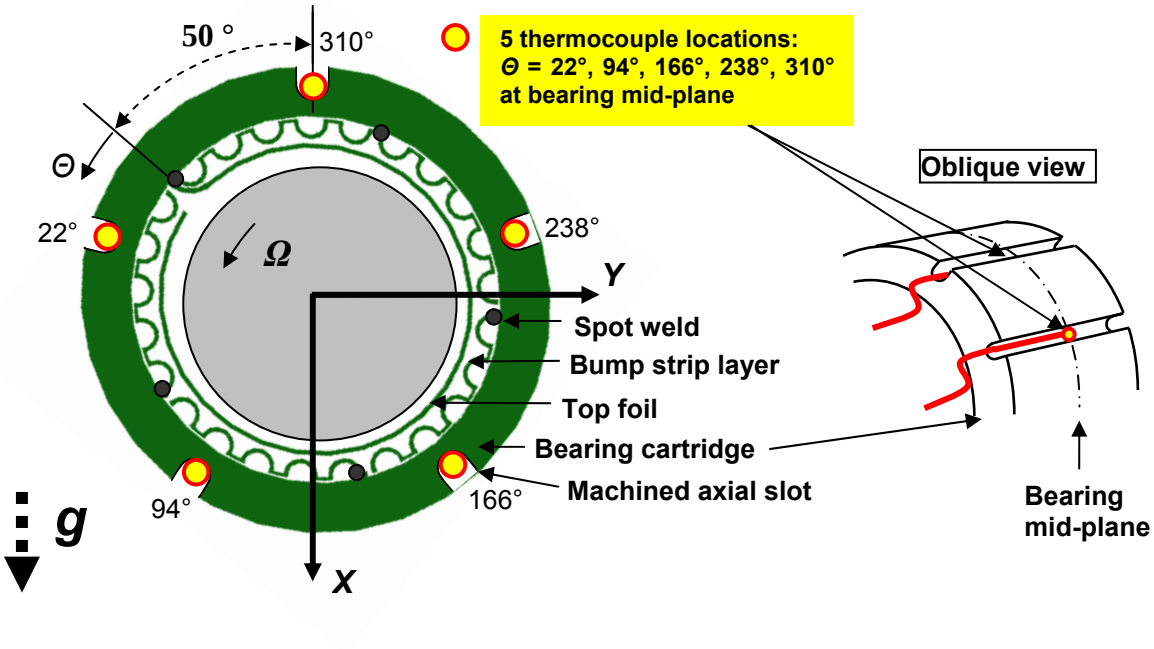

Figure 3. Schematic representation of test bump-type foil gas bearing with five (5) thermocouples placed in machined axial slots. Five (5) temperature measurement locations (Θ = 22°, 94°, 166°, 238°, 310°) at bearing mid plane

Temperature measurements are recorded during rotor operation at increasing speeds up to 26 krpm for increasing set temperatures of the heater (T_c = 22 °C, 93 °C, and 132 °C), without and with axial cooling air flow. The room ambient temperature T_a ~ 22 °C. Table 1 describes test cases 1-6 for increasing heater temperatures (T_c) and cooling conditions. Case sets 1-3 and 4-6 represent rotor operations without and with cooling flow (~ 56 liter/min), respectively, for the

2 The test GFB consists of a single arcuate top foil and five corrugated bump strip layers. The leading edge of the top foil is free, while its trailing edge is spot welded to the bearing housing. Beneath the top foil, the five bump strip layers, each with five bumps, are split into five axial segments. One end of the bump strip layers is spot welded to the bearing housing while the other end is free. The orientation of the top foil spot-weld with respect to the vertical (gravity) plane is noted [17].

cartridge temperatures T_c = 22 °C, 93 °C, and 132 °C. Temperature measurements are taken manually in steady state temperature condition at each rotor speed. Table 1 also shows the total number of test hours to reach steady state operating temperatures for each test case.

Table 1. Description of test cases for three heater temperatures (T_c) and cooling conditions

	Test No. (test hours)**	Parameter*	Value			
Without cooling flow	Case 1 (5h 37m)	Rotor speed [krpm]	8	16	21	26
		Heater temperature [°C]	22	→	→	→
	Case 2 (7h 47m)	Rotor speed [krpm]	8	16	21	26
		Heater temperature [°C]	93	→	→	→
	Case 3 (5h 56m)	Rotor speed [krpm]	8	16	21	26
		Heater temperature [°C]	132	→	→	127†
With cooling flow	Case 4 (4h 35m)	Rotor speed [krpm]	8	16	21	26
		Heater temperature [°C]	22	→	→	→
		Cooling flow [L/min]	56	→	→	→
	Case 5 (8h 37m)	Rotor speed [krpm]	8	16	21	26
		Heater temperature [°C]	93	→	→	→
		Cooling flow [L/min]	56	→	→	→
	Case 6 (5h 20m)	Rotor speed [krpm]	8	16	21	26
		Heater temperature [°C]	132	→	→	127†
		Cooling flow [L/min]	56	→	→	→

* Uncertainties for thermocouples and flow meter are ± 0.28 °C and ± 0.05 L/min, respectively.
** Time of operation to establish steady state temperatures.
† Cartridge heater maximum heating temperature reduces from 132 °C at ~21 krpm to 127 °C at 26 krpm.

V. STEADY STATE TEMPERATURE MEASUREMENTS DURING ROTOR OPERATION AT INCREASING ROTOR SPEEDS

Figure 4 shows the temperature ratio $(T_{DBi} - T_a)/T_a$ versus rotor speed for increasing heater temperatures (T_c). (T_{DBi}) is the temperature measured at the drive end bearing cartridge (mid-plane). The ambient temperature T_a ~ 22 °C[3]. A cross-section view of the test rig (drive end) shown on the right depicts the location of temperature measurement; see also Fig. 3. Note that four other thermocouples installed around the bearing circumference are not shown in the view. The figure shows temperatures ratios for mean temperatures (or arithmetical averages) from five measurements, maximum temperatures, and minimum temperatures. Note that differences in the temperature ratio at five locations are attributed to the differences in the heater surface temperatures along its circumference. In Appendix B, the mean heater temperatures from five measurements taken along the heater circumference has a maximum standard deviation as large as 11 °C at T_c = 93 °C, for example. Appendix C provides the temperature ratio at each circumferential location as the rotor speed increases from 0 rpm to 26 krpm at T_c = 93 °C.

The temperature ratios increase, as the heater temperature increases and as the rotor speed increases. In cases 4-6, an axial cooling flow (Q ~56 liter/min) decreases the bearing temperature effectively, in particular for rotor operation without heating, i.e., T_c = 22 °C, and at the low speed of 8 krpm.

Figure 5 shows the temperature ratio $(T_{DBo} - T_a)/T_a$ versus rotor speed for increasing heater temperatures (T_c). (T_{DBo}) is the temperature measured at the drive end bearing outer surface. See also Fig. 3 for the location of temperature measurement. The temperature (T_{DBo}) shows similar trends to (T_{DBi}) shown in Fig. 4, albeit with lower magnitudes, in particular for the largest heater temperature T_c = 132 °C. The decrease in temperature is due to the heat flows conducted to the bearing support through the bearing cartridge and also convected to ambient on the sides of the bearing.

3 Ambient temperature varies slightly during tests. The mean temperature Ta ~ 21.7 °C with a standard deviation of 0.7 °C

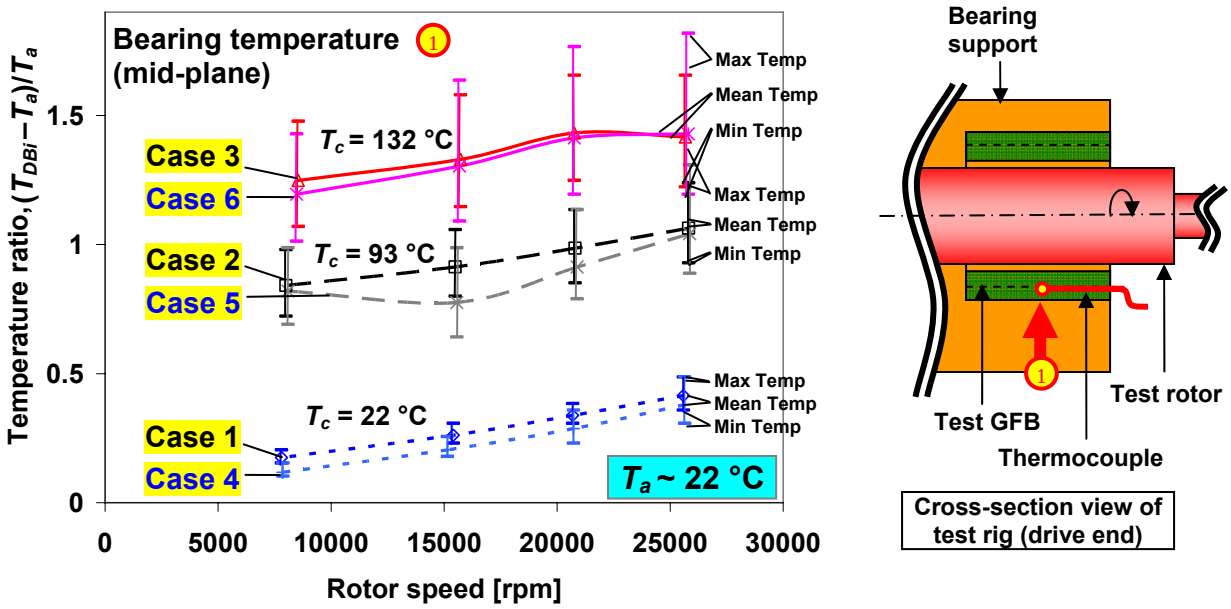

Figure 4. Temperature ratio $(T_{DBi} - T_a)/T_a$ versus rotor speed for three heater temperatures (T_c). (T_{DBi}) measured at drive end bearing cartridge (mid-plane)

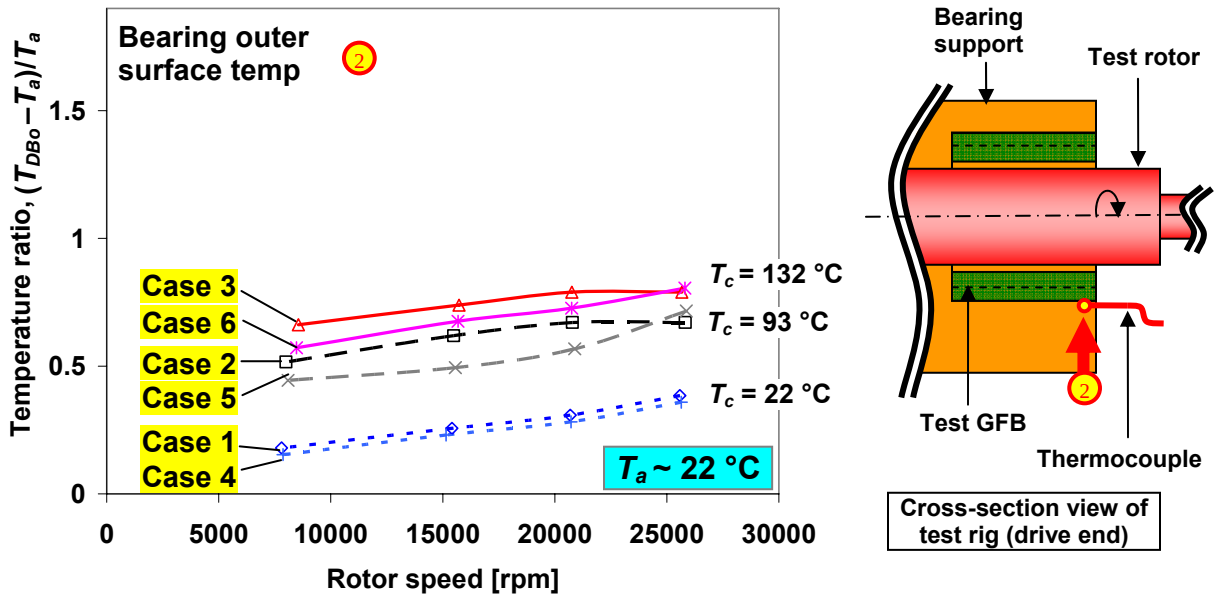

Figure 5. Temperature ratio $(T_{DBo} - T_a)/T_a$ versus rotor speed for three heater temperatures (T_c). T_{DBo} measured at drive end bearing outer surface

Figure 6 shows the temperature ratio $(T_{DS} - T_a)/T_a$ versus rotor speed for increasing heater temperatures (T_c). Temperature (T_{DS}) is measured at the rotor drive end. See also Fig. 3 for the location of temperature measurement. The temperature (T_{DS}) shows similar trends to those in Fig. 5 for (T_{DBo}), but with slightly larger magnitudes, in particular for the highest heater temperature T_c = 132 °C. Note that the rotor temperature is measured at the drive end, i.e., not at a bearing location, thus showing lower temperatures than those for the inner bearing cartridge temperatures.

Figure 7 shows the temperature ratio $(T_{DBS} - T_a)/T_a$ versus rotor speed for increasing heater temperatures (T_c). (T_{DBS}) is measured at the bearing support drive end. The temperatures are much higher than those for the rotor drive end, see Fig. 6. Heat flowing into the bearing support by conduction through the drive end GFB may increase the bearing support temperature. The axial cooling flow (Q ~56 liter/min) acts to decrease the bearing support temperature. This is more pronounced than those (for T_{DBi}, T_{DBo}, T_{DS}) shown in Figs. 4-6, because the cooling flow forced at the center of the test rig carries away heat (from the hot shaft) along the whole axial length of the bearing support (see Fig. 2).

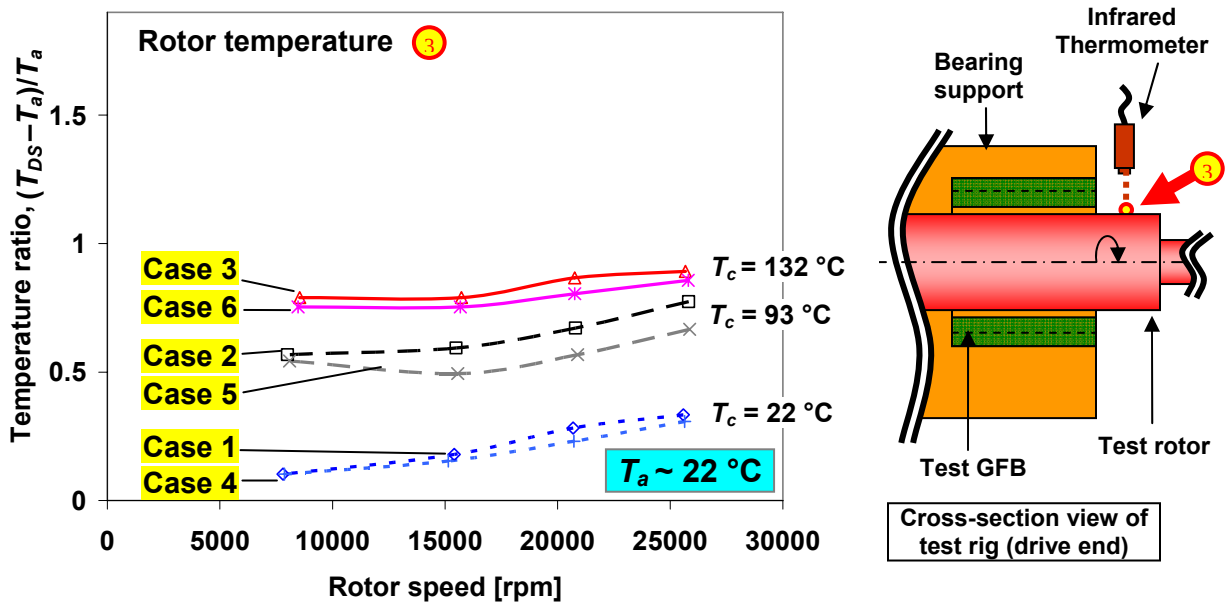

Figure 6. Temperature ratio $(T_{DS} - T_a)/T_a$ versus rotor speed for three heater temperatures (T_c). (T_{DS}) measured at rotor drive end

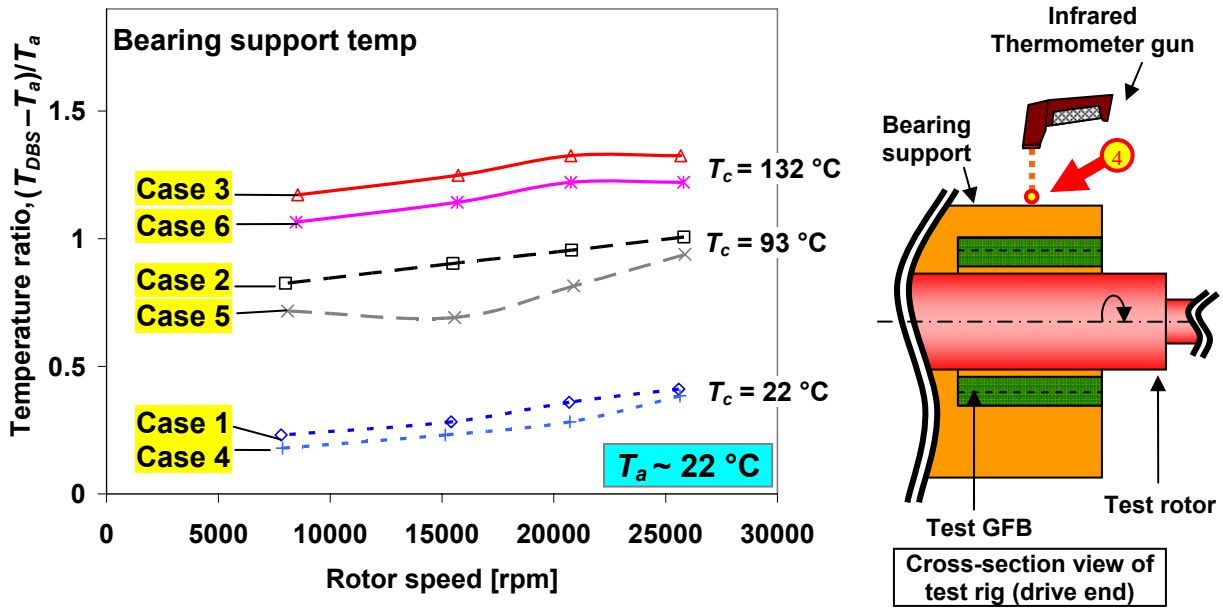

Figure 7. Temperature ratio $(T_{DBS} - T_a)/T_a$ versus rotor speed for three heater temperatures (T_c). (T_{DBS}) measured at bearing support drive end

Figure 8 shows the temperature ratio $(T_k-T_a)/T_a$ versus rotor speed for temperatures measured at various locations (1-4); where k = *DBi, DBo, DS,* and *DBS.* No axial flow is supplied for operation without shaft heating, i.e., T_c = 22 °C (case 1). Note the vertical axis in a different scale from those in Figs. 4-7. In general, all temperatures (bearing cartridge, bearing outer surface, bearing support, and rotor surface) show similar values with differences in magnitude < 0.2 at each rotor speed. The temperatures increase as the rotor speed increases.

Appendix D shows the rotor whirl orbits at 26 krpm and trajectories of the rotor center at increasing rotor speeds for Cases 1 – 3. In general, as the heater temperature increases from 22 °C to 132 °C, the rotor orbit size at 26 krpm increases slightly and the trajectories of the rotor center move up slightly.

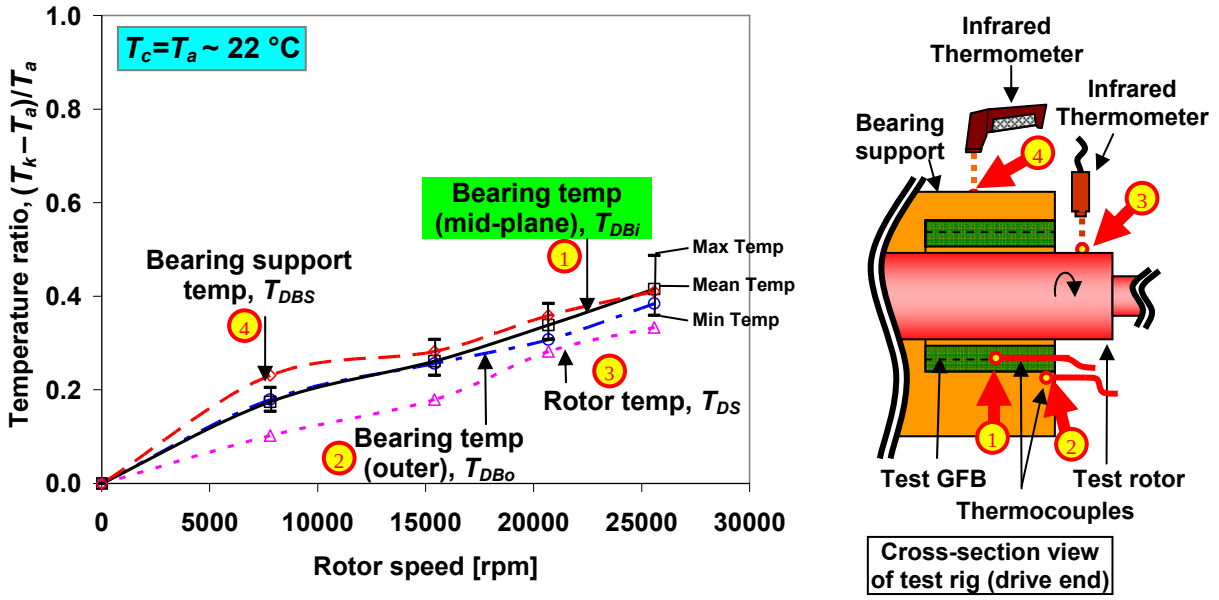

Figure 8. Temperature ratio $(T_k-T_a)/T_a$ versus rotor speed for temperatures measured at various locations (1-4). $T_c = T_a$ ~ 22 °C (case 1). No axial cooling flow

VI. ROTORDYNAMIC PERFORMANCE OF A ROTOR SUPPORTED ON GFBS FOR INCREASING HEATER TEMPERATURES (T_C).

For three cartridge heater temperatures (T_c) and without a cooling flow, Fig. 9 presents rotor amplitude of synchronous response recorded during rotor speed-up tests to 26 krpm. See Table 1, cases 1-3. The measurements are taken at the rotor (a) drive and (b) free ends, vertical plane without added imbalance masses while the rotor speed manually increases to 26 krpm. Slow roll compensations at 2.3 krpm exclude the rotor run-out amplitudes.

Without shaft heating (T_c = T_a = 22 °C), the rotor motion shows peaks in amplitude at the critical speed of 14.5 krpm. For rotor speed just above the critical speed, the amplitude drops suddenly, thus implying a nonlinearity. Recall that a strong hardening effect of a GFB elastic structure results in a nonlinear rotor-bearing system response behavior [17]. As T_c increases to 132 °C, the peak amplitude decreases dramatically without amplitude jump for operation above the critical speed.

For three cartridge heater temperatures (T_c) and without a cooling flow, Fig. 10 presents the rotor amplitude of synchronous response recorded during rotor coastdown tests from 26 krpm. The measurements are taken at the rotor (a) drive and (b) free ends, vertical plane without added

imbalance masses. Slow roll compensations at 2.3 krpm exclude the rotor run-out amplitudes. Without shaft heating (T_c = T_a = 22 °C), the rotor shows a peak amplitude at a critical speed ~ 11.5 krpm. As T_c increases to 132 °C, the critical speed increase to ~13 krpm and the peak amplitude decreases significantly without amplitude jump behavior. Appendix E shows the rotor phase angle of synchronous response and rotor direct (synchronous) amplitude without slow roll compensations, recorded during rotor coastdown tests from 26 krpm without a cooling flow for cases 1-3. Note that rotor direct (synchronous) amplitude jumps up near the critical speed at T_c = T_a = 22 °C, while it does not at T_c = 132 °C, as in Fig. 11.

Figure 11 display waterfall plots of direct rotor amplitude of synchronous response for increasing cartridge heater temperatures (T_c) recorded during rotor coastdown tests from 26 krpm without a cooling flow. The measurements are the rotor free end, vertical plane without added imbalance masses. The lines labeled 1X denote synchronous rotor motions. Subsynchronous and super synchronous motions are negligibly small over the whole test speed range.

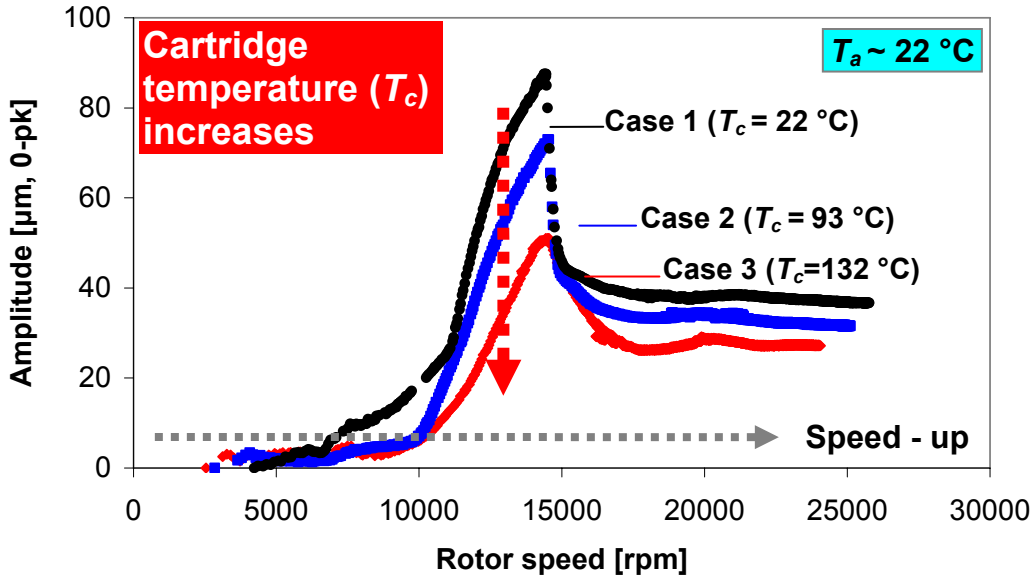

(a) Rotor drive end, vertical plane

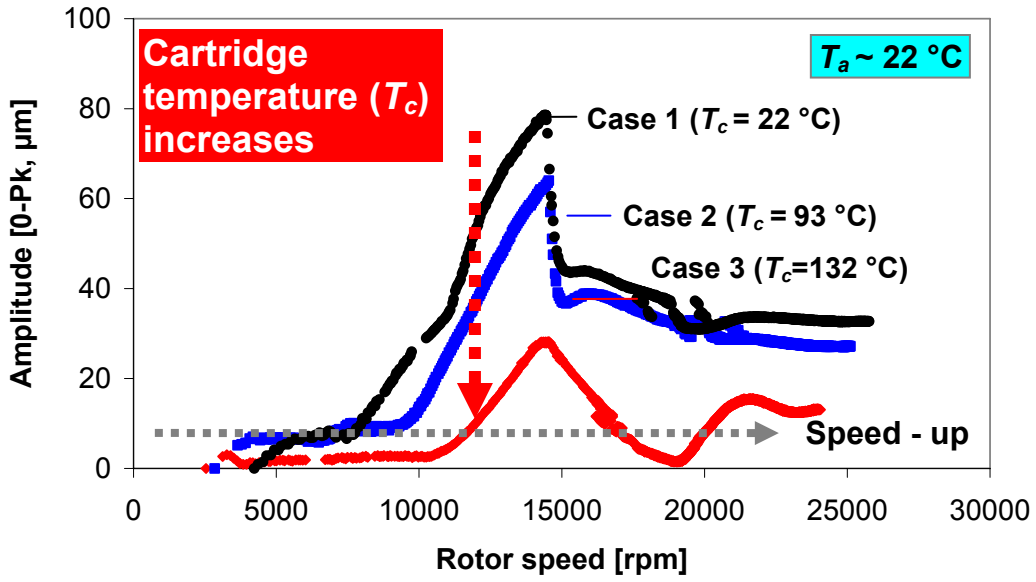

(b) Rotor free end, vertical plane

Figure 9. Rotor amplitude of synchronous response for three heater cartridge temperatures (T_c). Rotor speed-up tests to 26 krpm. Test cases 1-3. Slow roll compensations at 2.3 krpm. Rotor (a) drive and (b) free ends, vertical plane. No axial cooling flow

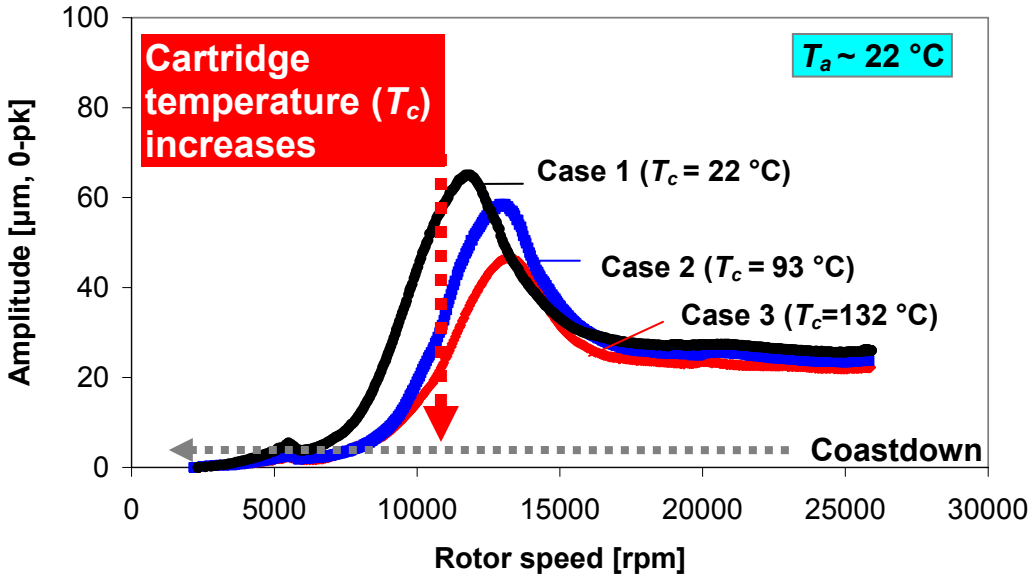

(a) Rotor drive end, vertical plane

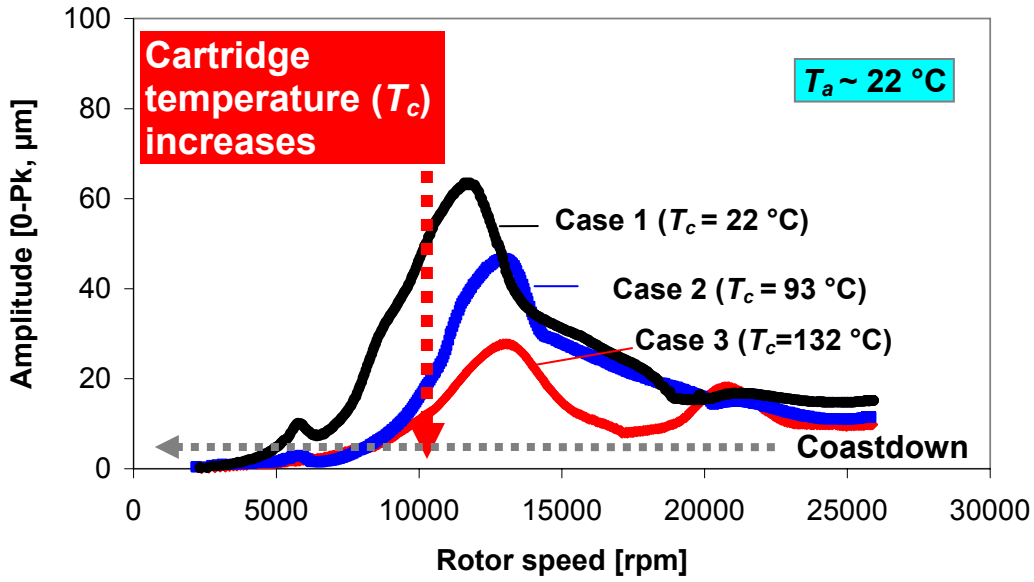

(b) Rotor free end, vertical plane

Figure 10. Rotor amplitude of synchronous response for three heater cartridge temperatures (T_c). Rotor coastdown tests from 26 krpm. Test cases 1-3. Slow roll compensations at 2.3 krpm. Rotor (a) drive and (b) free ends, vertical plane. No axial cooling flow

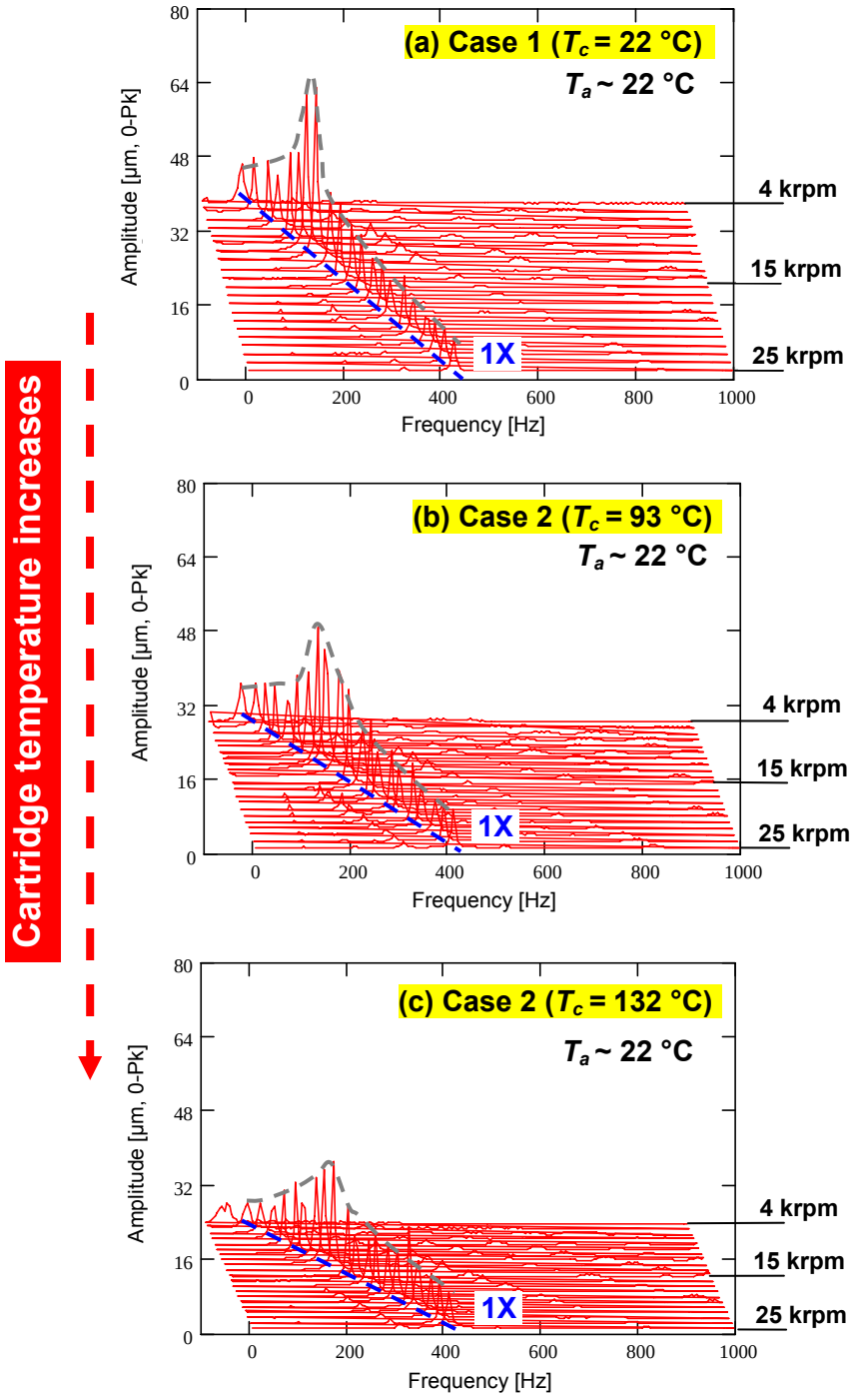

Figure 11. Waterfalls of coast down rotor response from 26 krpm for three heater cartridge temperatures (T_c). Rotor coastdown tests from 26 krpm. Test cases 1-3. Rotor free end, vertical plane. No axial cooling flow.

For three cartridge heater temperatures (T_c) and without cooling flow, Fig. 12 displays the rotor coastdown speed versus time. In general, all results display an exponential decay of rotor speed with time from 26 krpm to ~ 8 krpm, thus revealing operation with "viscous" drag. However, in all cases, the decay rate of rotor speed changes at ~ 15 krpm (near the critical speeds). The largest rotor amplitude for case 1 (T_c=T_a) causes the most significant change in speed decay rate, thus leading to the shortest coastdown time. From ~7 krpm until rest, rotor operation shows dry friction effects (rotor rub) with a fast deceleration to rest for case 1. Note that the rotor has the highest touchdown (rotor rub) speed ~9 krpm for case 3 (T_c=132 °C). See Appendix F for the coastdown rotor speed in a linear scale.

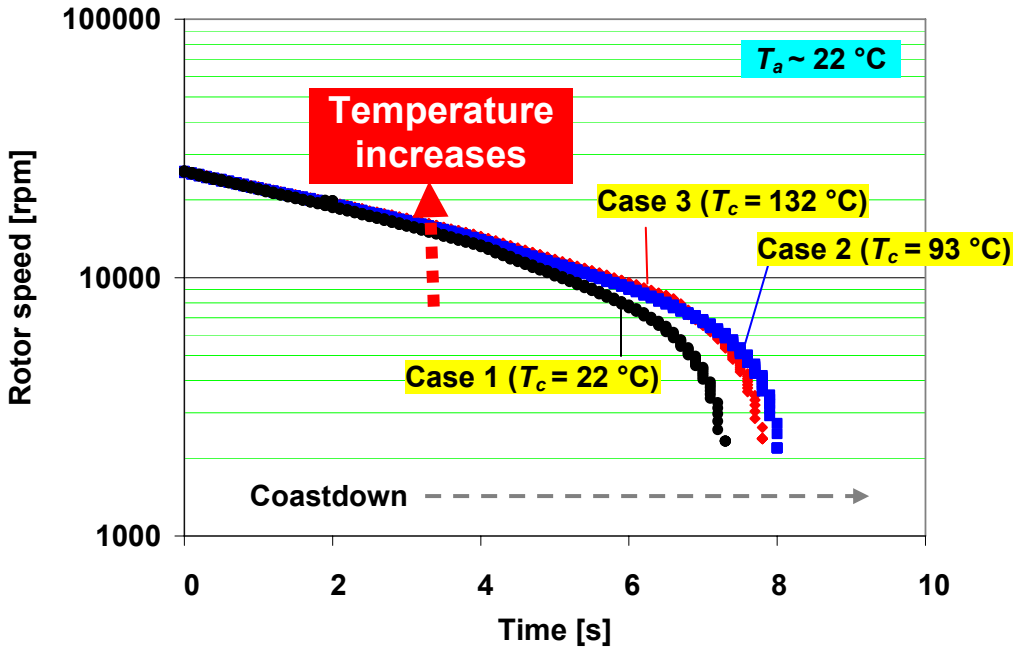

Figure 12. Rotor coastdown speed versus time for three heater cartridge temperatures (T_c). Rotor coastdown tests from 26 krpm. Test cases 1-3. No axial cooling flow

VII. CONCLUSIONS

The GFB rotordynamic test rig was revamped with an electric cartridge heater, loosely fitted inside the hollow rotor. K-type thermocouples measure temperatures of two test GFBs, and infrared thermometers record surface temperatures of the rotating shaft and the bearing support (housing). Test results show the GFB cartridge temperatures increase, as the heater temperature increases and as the rotor speed increases. An axial cooling flow (Q ~56 liter/min) decreases the temperature, but only by ~5 %.

Heater temperatures, as high as 130 °C, are set in the system. Long times, on the order of hours, are required to reach thermal steady state condition. The tests show the bearing temperatures increase as the heater temperature increases and as the rotating speed increases. Rotor speed-up tests without shaft heating reveal the rotor amplitude drops suddenly just above its critical speed, thus implying nonlinear system response. As the rotor temperature increases, the rotor amplitudes of motion decrease and show no jumps. During rotor speed coastdown tests, the critical speed increases slightly as the heater temperature increases. Waterfall plots of the direct rotor amplitude of synchronous response show dominant synchronous rotor motions. During coastdowns, the rotor speed decays exponentially with time from 26 krpm to ~ 8 krpm, in general, thus evidencing operation with “viscous” drag. However, in all cases, the decay rate of rotor speed changes at ~ 15 krpm (near the critical speeds).

VIII. REFERENCES

[1] DellaCorte, C., and M., Valco, 2000, “Load Capacity Estimation of Foil Air Journal Bearing for Oil-Free Turbomachinery Applications,” STLE Tribol. Trans., **43**(4), pp. 795-801.

[2] Agrawal, G. L., 1997, “Foil Air/Gas Bearing Technology – an Overview,” ASME Paper No. 97-GT-347.

[3] Lubell, D., DellaCorte, C. and Stanford, M., 2006, “Test Evolution and Oil-Free Engine Experience of a High Temperature Foil Air Bearing Coating,” ASME Paper No. GT2006-90572.

[4] Radil, K., DellaCorte, C., Bruckner, R., and Zessoteck, M., 2007, “Thermal Management Techniques for Oil-Free Turbomachinery Systems,” STLE Tribol. Trans., **50**, pp. 319-327.

[5] Bauman, S., 2005, “An Oil-Free Thrust Foil Bearing Facility Design Calibration, and Operation,” NASA/TM-2005-213568.

[6] Heshmat, H., Tomaszewski, M. J., and Waltono, J. F., 2006, “Small Gas Turbine Engine Operating with High-Temperature Foil Bearings,” ASME Paper No. GT2006-90791.

[7] San Andrés, L., 2007, “Prediction of Foil bearing Performance: a Computational Model Anchored to Test Data,” Proposal submitted to NASA SSRW2-1.3 Oil Free Engine technology Program, April.

[8] DellaCorte, C., 1997, “A New Foil Air Bearing Test Rig for Use to 700 ºC and 70,000 rpm,” NASA TM-107405.

[9] DellaCorte, C., Valco, M. J., Radil, K. C., and Heshmat, H., 1999, “Performance and Durability of High Temperature Foil Air Bearings for Oil-Free Turbomachinery,” NASA/TM-1999-209187.

[10] DellaCorte, C., Zaldana, A., and Radil, K., 2003, “A System Approach to the Solid Lubrication of Foil Air Bearing for Oil-Free Turbomachinery,” ASME J. Tribol., **126**(1), pp. 200-207.

[11] Howard, S., DellaCorte, C., Valco, M.-J., Prahl, J.-M., and Heshmat, H., 2001, “Steady-State Stiffness of Foil Air Journal Bearings at Elevated Temperatures,” STLE Tribol. Trans., **44**(3), pp. 489-493.

[12] Howard, S., DellaCorte, C., Valco, M.-J., Prahl, J.-M., and Heshmat, H., 2001, “Dynamic Stiffness and Damping Characteristics of a High-Temperature Air Foil Journal Bearing,” STLE Tribol. Trans., **44**(4), pp. 657-663.

[13] Lee, Y.-B., Jo, J.-H., Park, D.-J., Kim, C.-H., and Rhim, Y.-C., 2006, “Dynamic Characteristics of Bump Foils Considering with Thermal Effect in Air Foil Bearings,” ASME Paper No. IJTC2006-12189.

[14] Salehi, M., Swanson, E., and Heshmat, H., 2001, “Thermal Features of Compliant Foil Bearings – Theory and Experiments,” ASME J. Tribol., **123**, pp. 566-571.

[15] San Andrés, L., Rubio, D., and Kim, T.H, 2007, “Rotordynamic Performance of a Rotor Supported on Bump Type Foil Gas Bearings: Experiments and Predictions,” ASME J. Eng. Gas Turbines Power, **29**(3), pp. 850-857.

[16] Kim, T. H., 2007, “Analysis of Side End Pressurized Bump Type Gas Foil Bearings: A Model Anchored to Test Data,” Texas A&M University, Ph. D. Dissertation, College Station, TX.

[17] Kim, T.H, and San Andrés, L., 2008 “Effect of Side End Pressurization on the Dynamic Performance of Gas Foil Bearings – A Model Anchored to Test Data,” ASME Paper No. GT2008-50571.

[18] San Andrés, L., and Kim, T. H., 2008, “Forced Nonlinear Response of Gas Foil Bearing Supported Rotors,” Tribol. Intl., 41(8), pp. 704-715.

[19] Rubio, D. and San Andrés, L., 2003, “Bump-Type Foil Bearing Structural Stiffness: Experiments and Predictions,” Technical report TRC-B&C-5-03, Texas A&M Univ. College Station, TX.

APPENDIX A: ORIGINAL AND REBUILT FOSTER-MILLER FOIL BEARINGS

In 2007, two foil bearings were *damaged* due to inappropriate usage. The bearing manufacturer (Foster-Miller Technologies, Inc) rebuilt the bearings at a cost of $3,000. The repaired bearings have no coating applied to the top foil, and thus could be used in high temperature tests. Figure A1 shows pictures of a repaired foil bearing, and Table A1 lists the measured (nominal) dimensions of the two repaired foil bearings (GFB3 and GFB4). Table A1 also includes the dimensions of two original foil bearings GFB1 and GFB2, (Teflon® coated) [18]. Presently, GFB1 (coated) and GFB3 (uncoated) are installed at the test rig drive and free ends, respectively; see Fig. 1.

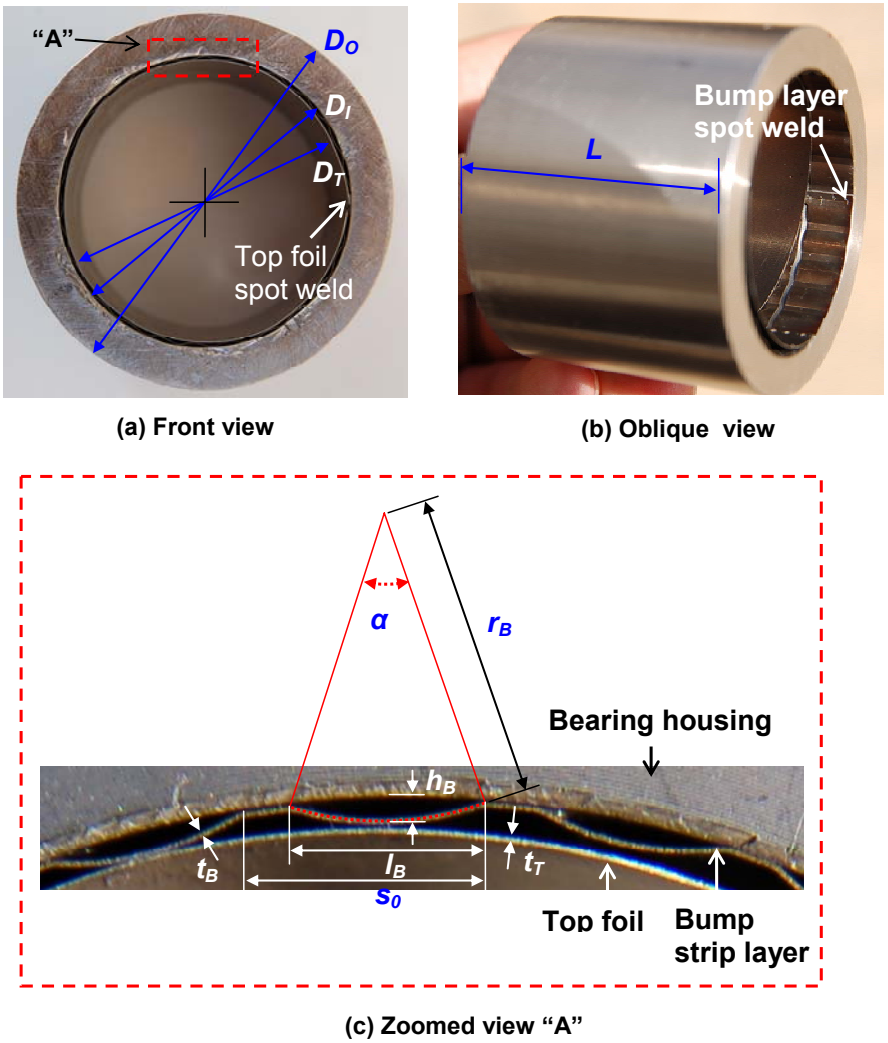

(a) Front view

(b) Oblique view

(c) Zoomed view "A"

Figure A1. Repaired Foster Miller foil gas bearing and its dimensions

Table A1. Measurement of test foil bearing nominal dimensions (Unit: mm). Foster Miller Foil Bearings

Parameters	GFB 1 (original [18])	GFB 2 (original [18])	GFB 3 (repaired)	GFB 4 (repaired)	Manufacturer Data [18]
Bearing housing outer diameter, D_O	51.04	51.02	50.85	50.82	-----
Bearing housing wall thickness, t_B	-----	-----	5.746	5.776	-----
Bearing housing inner diameter, $D_I = D_O - 2\ t_B$	-----	-----	39.36	39.27	-----
Bearing housing axial length, L	38.34	38.23	38.20	38.14	----
Top foil thickness, t_T	0.157	0.157	0.10	0.10	0.102
Bump foil thickness, t_B	N/A	N/A	0.10	0.10	0.1016
Number of Bumps, N_B	25	25	25	25	25
Bump pitch, s_0 (deg)	4.635 (13)	4.628 (13)	4.581* (13)	4.581* (13)	4.572
Bump length, l_B	4.064	4.064	3.742* (3.76)	3.742* (3.80)	N/A
Bump height, h_B	N/A	N/A	0.387* (0.484)**	0.387* (0.484)**	0.381
Bump arc radius, r_B	-----	-----	5.581*	5.581*	-----
Bump arc angle, α (deg)	-----	-----	36.5*	36.5*	-----
Poisson's Ratio	N/A	N/A	N/A	N/A	0.29
Modulus of Elasticity (Pa)	N/A	N/A	N/A	N/A	213736.4
Inner Diameter, D_T	38.35	38.31	38.19	38.10	38.17
Nominal Clearance[4]	N/A	N/A	N/A	N/A	0.0355

* Estimations from zoomed photos of Fig. A1.

** Bump height with consideration of the curvature of the bearing housing. See Figure A1.

[4] Nominal Clearance for a shaft diameter of 1.500 in

APPENDIX B: CALIBRATION OF ELECTRIC CARTRIDGE HEATER, MEASURED SURFACE TEMPERATURES OF HEATER AND HOLLOW SHAFT, AND SHAFT SURFACE CONDITIONS

The cartridge heater is calibrated in room temperature environment (~ 22°) using a thermocouple (Type K) fixed on the one end of the heater and an infrared thermometer measuring the heater surface temperatures along the axial length. The thermocouple provides a nominal heater temperature to the controller.

Figure B1 shows temperature measurements of the heater surfaces along the axial locations. The thermocouple fixed at Z = 10 mm shows the controlled temperatures (T_c = 22 °C to 93 °C) for the controller, and the infrared thermometer provides measured surface temperatures[5] along the axial length. Note that the figure shows mean temperatures from five measurements at every 72 ° along the heater circumference. The maximum standard deviation is as large as 10.7 °C at T_c = 93 °C. In general, the measured heater surface temperature changes as the axial location (X) increases. Peak temperatures occur at Z ~ 70 mm, for example.

Figure B2 presents temperature measurements of the hollow shaft surface along the axial length after the cartridge heater is installed within the stationary hollow rotor with a gap of 1.7 mm. Thermocouples fixed at Z = 10 mm give the controlled heater temperatures and the infrared thermometer provides the shaft surface temperatures[1] along the axial cartridge length. The figure shows mean temperatures from three measurements at angles separated by 120 ° around the shaft circumference. The maximum standard deviation is as large as 16 °C at T_c = 93 °C. An increase in the heater temperature increases effectively the shaft surface temperature. While the shaft has peak temperatures at Z ~ 60 mm, it has significantly lower temperatures around Z ~ 80 mm and Z~ 190 mm where the bearing location on the shaft is thin dense Chrome coated[6] for high temperature operation. Note that the heater and shaft temperature are calibrated up to the peak temperature ~200 °C since the present rotordynamic test rig uses eddy current sensors which have maximum operating temperature of 177 °C[7]. Note also that Ref. [1] details the eddy current

[5] Three measurements are taken at angles separated by 120 ° around the heater and shaft circumferences, and those are averaged in Figs. 2 and 3.

6 The high temperature shaft coating (>500 °C) is donated by Multichrome/Microplate Certified Processing Lab, Inc. (http://www.multiplate.com/)

7 High temperature optical displacement sensors will replace eddy current sensors for operation at higher temperatures during next research year 2008-2009.

sensor calibration for increasing temperatures which shows nearly constant gains with standard deviation ~ 0.77% between 22 °C and 121 °C.

Figure B3 shows the shaft surface conditions (a) before and (b) after the heating tests up to the peak temperature T_{cp} ~200 °C. Heating the shaft causes discoloration on the shaft surface. As the axial location (or the measured shaft surface temperature) increases, the shaft surface color changes, thus implying that a careful inspection of the discoloration may guess the shaft temperature distribution.

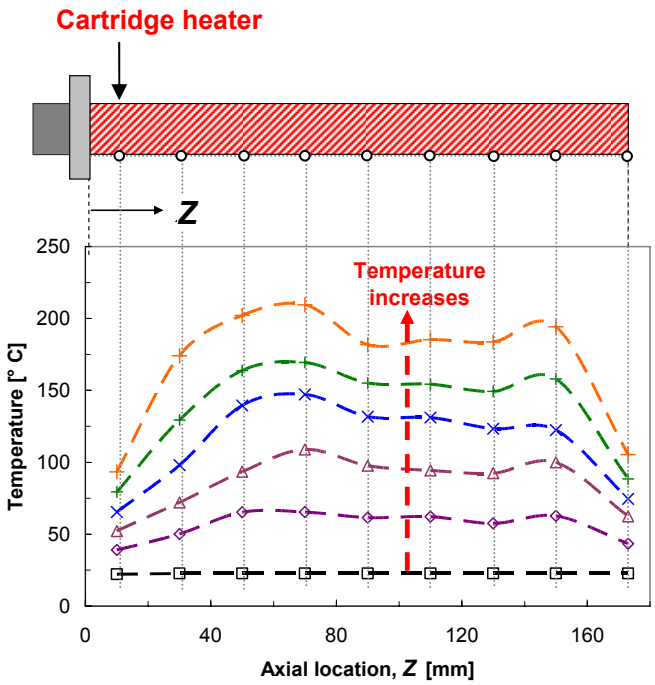

Figure B1. Measured surface temperature on electric heater versus axial location for increasing controlled temperatures (T_c) at Z=10 mm. Ambient temperature (T_a) = 22 °C

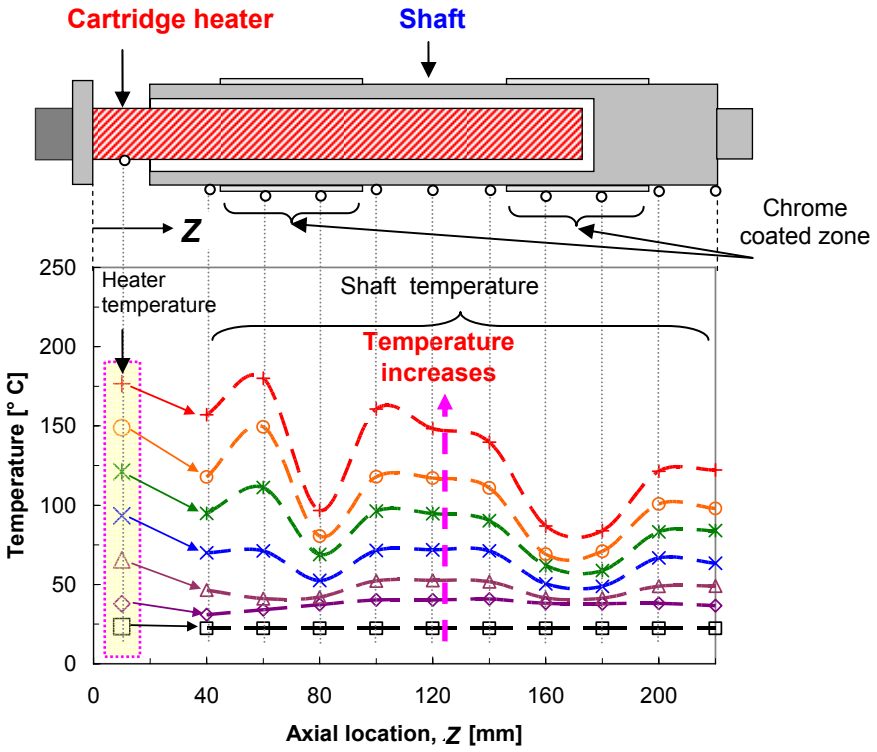

Figure B2. Measured outer shaft temperature versus axial location for increasing controlled heater temperatures (T_c) at Z=10 mm. Ambient temperature (T_a) = 22 °C

(a) Before heating

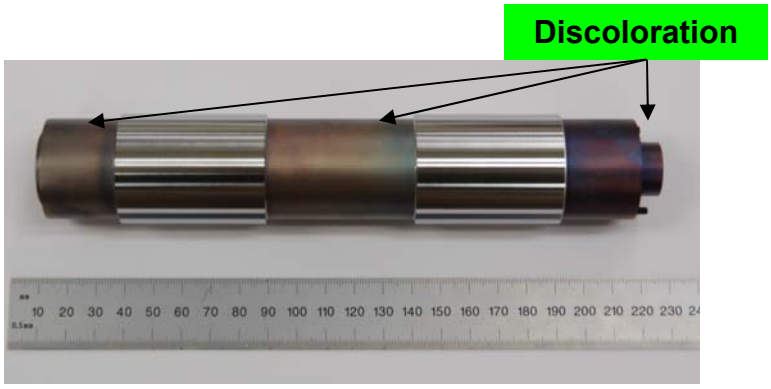

(b) After heating up to T_{cp} = 200 °C

Figure B3. Test rotor surface condition (a) before and (b) after heating up to to T_{cp} ~ 200 °C. Ambient temperature (T_a) = 22 °C

APPENDIX C: CIRCUMFERENTIAL BEARING CARTRIDGE TEMPERATURES FOR INCREASING ROTOR SPEEDS: TEST CASE 2

Figure C1 shows the temperature ratio $(T_{DB} - T_a)/T_a$ versus bearing circumferential location for increasing rotor speeds from 0 rpm to 26 krpm at a heater temperature T_c = 93 °C. No cooling air flow is supplied, i.e., Test case 2. The temperature ratios are different depending on the bearing circumferential location, even without rotor spinning. Recall that the heater mean temperatures from five measurements taken along the heater circumference have large standard deviations, see Appendix B. As the rotor spins, the temperatures at the bearing circumferential locations increase.

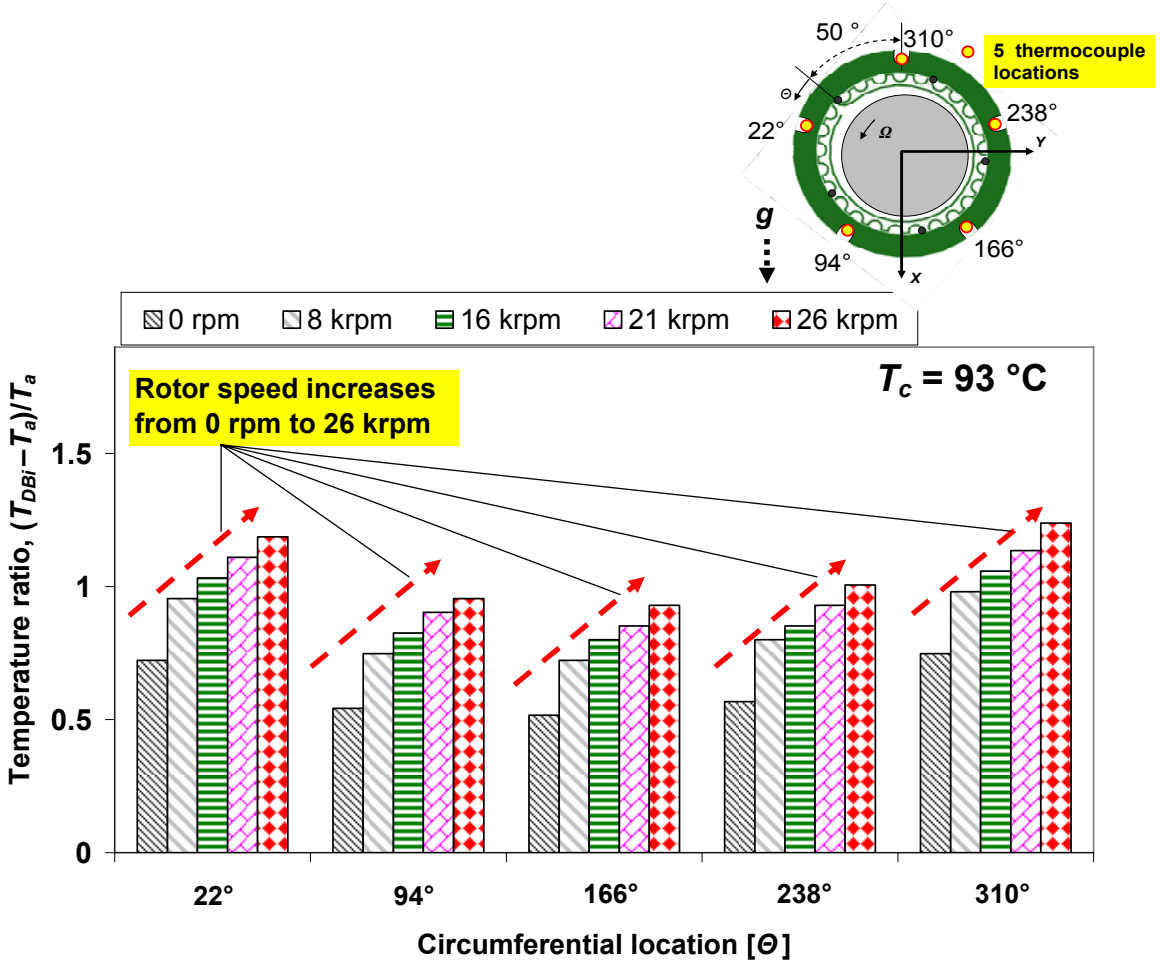

Figure C1. Temperature ratio $(T_{DBi} - T_a)/T_a$ versus bearing circumferential location for increasing rotor speeds from 0 rpm to 26 krpm. Heater temperatures T_c = 93 °C. Measurements at the drive end bearing cartridge (inner) for case 2. See also Fig. 2 for locations of temperature measurement

APPENDIX D: ROTOR WHIRL ORBITS AT 26 KRPM AND TRAJECTORIES OF ROTOR CENTER AT INCREASING ROTOR SPEEDS FOR TEST CASES 1 - 3

Figure D1 shows rotor whirl orbits at 26 krpm and trajectories of the rotor center at increasing rotor speeds for cases 1 – 3. The test data are recorded at the drive and free end bearing locations with DC-offset subtraction[8]. In general, as the heater temperature increases from 22 °C to 132 °C, the rotor orbit size at 26 krpm increases slightly and the trajectories of the rotor center move up slightly.

[8] Because the bearing geometric center, as well as the bearing clearance, are generally unknown, the initial rotor center position is set to zero (or origins in Fig. D1). In other words, the DC bottom line refers to the locations where the rotor is in contact with the test bearings and without rotor spinning

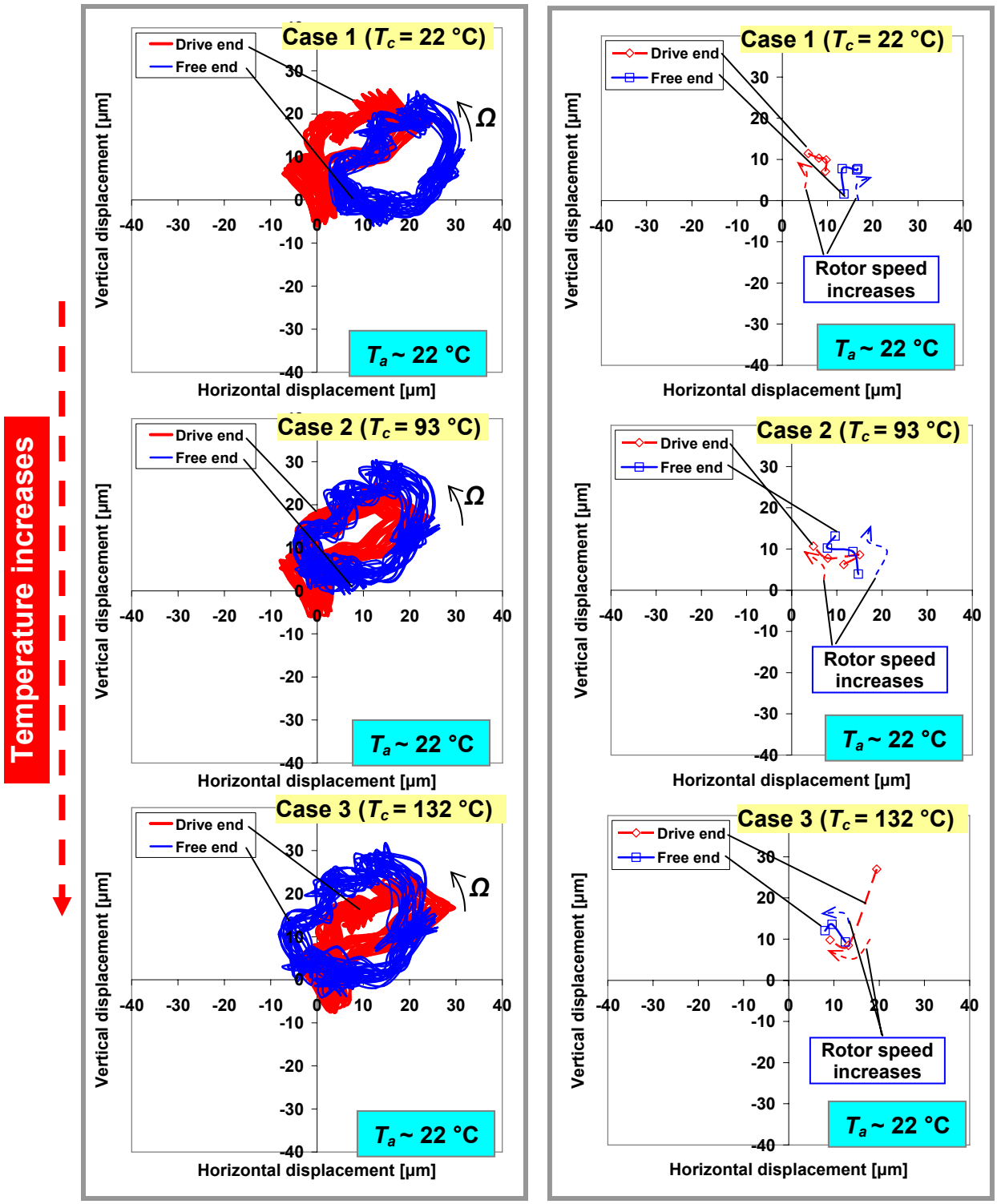

(a) Rotor whirl orbit at 25 krpm (b) Trajectory of rotor center

Figure D1. (a) Rotor whirl orbits at 25 krpm and (b) trajectories of rotor center at increasing rotor speeds of 8 krpm, 16 krpm, 21 krpm, and 26 krpm for test Cases 1 - 3. Drive and free end bearing locations with DC-offset subtraction. No axial cooling flow

APPENDIX E: PHASE ANGLE OF SYNCHRONOUS RESPONSE AND ROTOR DIRECT (SYNCHRONOUS) AMPLITUDE DURING ROTOR COASTDOWN TESTS FROM 26 KRPM FOR CASES 1-3

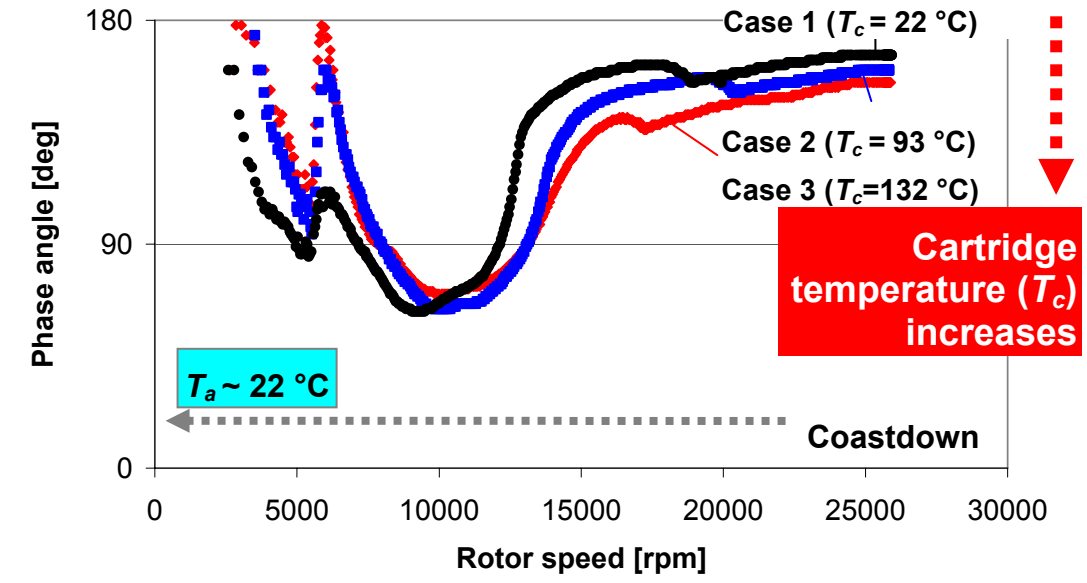

(a) Rotor drive end, vertical plane

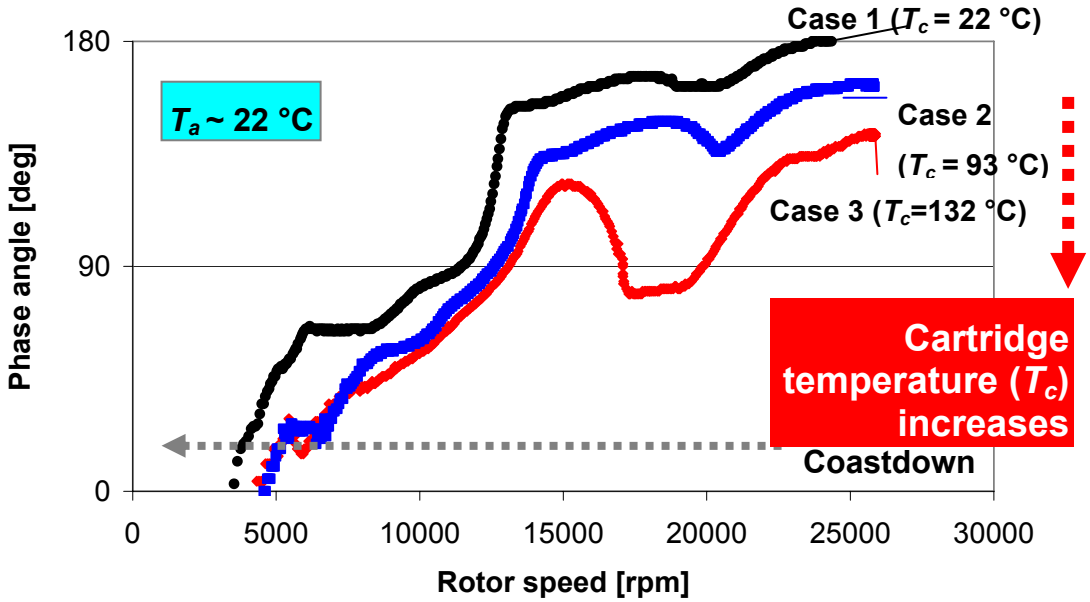

(b) Rotor free end, vertical plane

Figure E1. Rotor phase angle of synchronous response for three heater cartridge temperatures (T_c). Rotor coastdown tests from 25 krpm. Test cases 1-3. Slow roll compensations at 2.3 krpm. Rotor (a) drive and (b) free ends, vertical plane. No axial cooling flow

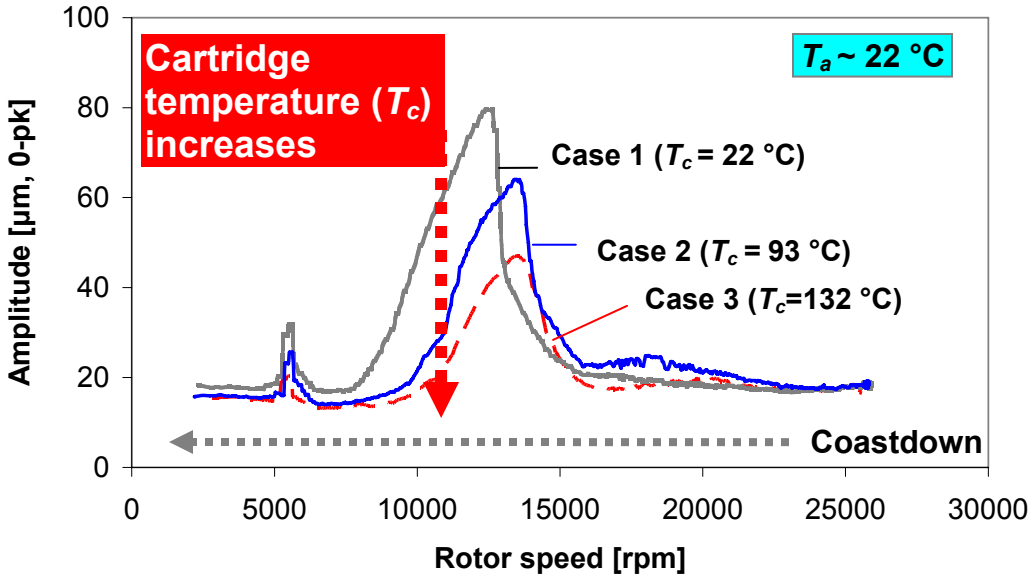

(a) Rotor drive end, vertical plane

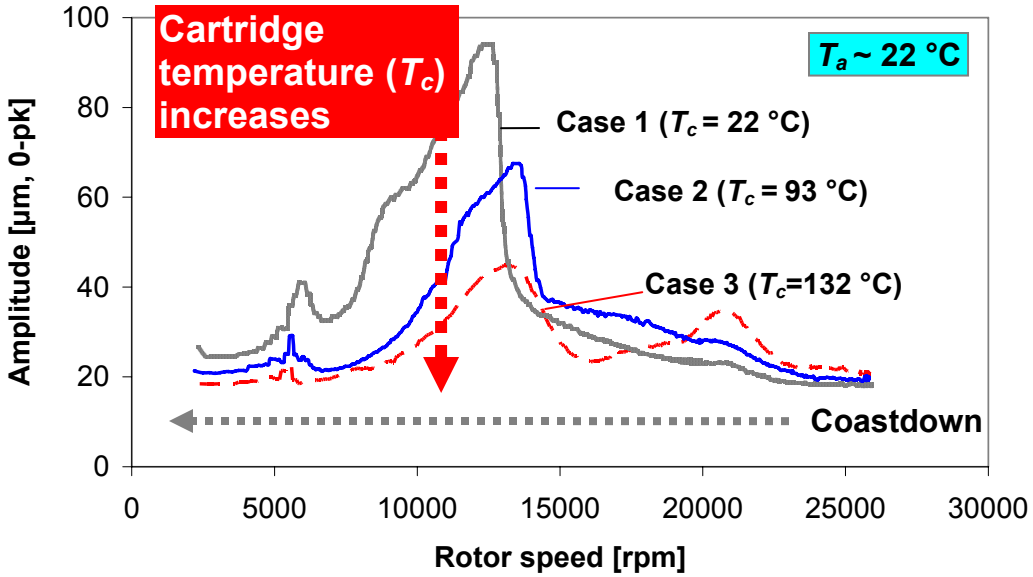

(b) Rotor free end, vertical plane

Figure E2. Rotor direct (synchronous) amplitude without slow roll compensation for three heater cartridge temperatures (T_c). Rotor coastdown tests from 26 krpm. Test cases 1-3. Rotor (a) drive and (b) free ends, vertical plane. No axial cooling flow

APPENDIX F: ROTOR SPEED (LINEAR SCALE) VERSUS TIME FOR THREE HEATER CARTRIDGE TEMPERATURES (T_C) DURING ROTOR COASTDOWN TESTS FROM 26 KRPM. TEST CASES 1-3

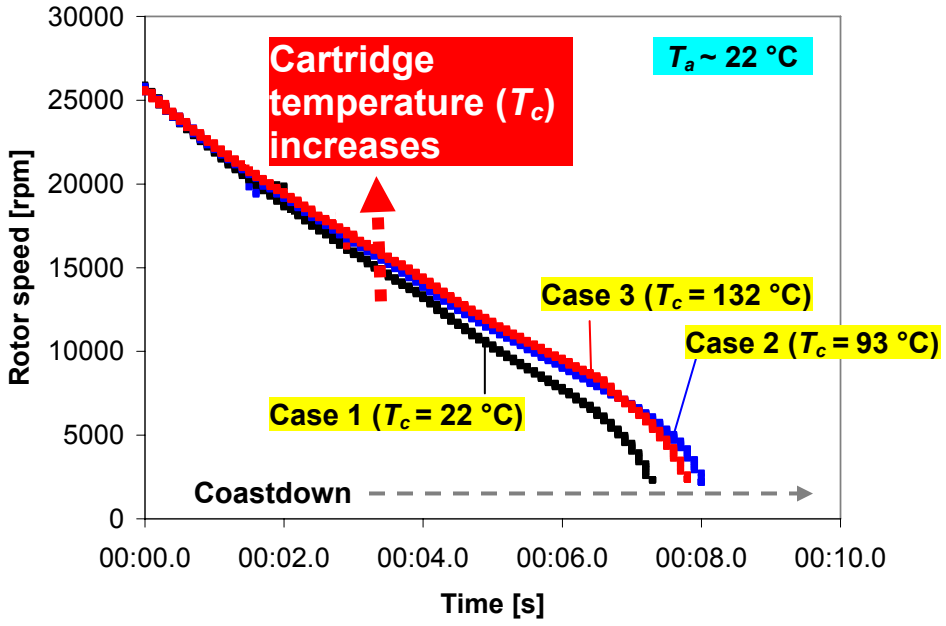

Figure F1. Rotor speed versus time for three heater cartridge temperatures (T_c). Rotor coastdown tests from 26 krpm. Test cases 1-3. No axial cooling flow